

Holographic Reflection Filters in Photorefractive LiNbO₃ Channel Waveguides

Detlef Kip and Jörg Hukriede

Osnabrück University, Physics Department, Barbarastrasse 7,
D-49069 Osnabrück, Germany,
Email: dkip@uos.de, jhukriede@uos.de

Abstract. Permanent refractive-index gratings in waveguide devices are of considerable interest for optical communication systems that make use of the high spectral selectivity of holographic filters, e.g., dense wavelength division multiplexing (DWDM) or narrow-bandwidth mirrors for integrated waveguide lasers in LiNbO₃. Other possible applications include grating couplers and optical sensors. In this contribution we investigate such holographic wavelength filters in Fe- and Cu-doped LiNbO₃ channel waveguides. Permanent refractive-index gratings are generated by thermal fixing of holograms in the waveguides. The samples are fabricated by successive in-diffusion of Ti stripes and thin layers of either Fe or Cu. After high temperature recording with green light, refractive-index changes up to $\Delta n \approx 10^{-4}$ for infrared light (1.55 μm) are obtained, resulting in a reflection efficiency well above 99 % for a 15 mm-long grating. Several gratings for different wavelengths can be superimposed in the same sample, which may enable more complex filters, laser mirrors or optical sensors. By changing the sample temperature the reflection wavelength can be tuned by thermal expansion of the grating, and wavelength filters can be switched on and off by applying moderate voltages using the electrooptic effect. Furthermore, we report on a new thermal fixing mechanism that does not need any additional development by homogeneous light illumination and therefore does not suffer from the non-vanishing dark conductivity of the material.

1 Introduction

Lithium niobate (LiNbO₃) crystals are promising substrate materials for applications in integrated optics because of their outstanding nonlinear properties, for instance the electrooptic, acoustooptic and photorefractive effect [1–3]. For any integrated circuit, channel waveguides are the basic elements, and high-quality waveguides with low damping constants can be fabricated in LiNbO₃ by, e.g., Ti in-diffusion or proton exchange [4–7]. By these techniques, devices such as waveguide lasers, directional couplers, mode converters, and fast light modulators have been realized [8–11].

LiNbO₃ can be doped with various metal impurities to tailor its photorefractive properties for holographic recording [12–14]. The most commonly used dopants are Fe and Cu. LiNbO₃:Fe and LiNbO₃:Cu crystals are sensitive to light in the visible green or blue wavelength region, but show only little effects in the red or near infrared spectral region. Especially in the 1.3 μm

and 1.55 μm wavelength band of optical communications no photorefractive effects have been observed for common continuous wave intensities. Doped LiNbO₃ volume crystals are usually produced by adding Fe₂O₃ or CuO to the melt during crystal growth. Nevertheless, it is also possible to increase the impurity concentration by in-diffusion of thin evaporated metal layers at high temperatures [15,16]. Here one can take advantage of the loosely-packed crystal structure of LiNbO₃, which results in relatively high diffusion constants of impurities in this material. The technique of diffusion doping is favorable for integrated optics because commercially available un-doped LiNbO₃ wafers may be used. A desired region can be locally doped, whereas the rest of the substrate remains unchanged.

For application of photorefractive crystals, a long-term stability of the device performance has to be guaranteed. However, phase holograms in these crystals suffer from destructive readout when the material is illuminated with light. In order to avoid erasure, different methods have been developed to make the recorded holograms insensitive for light. Interesting results have been obtained by two-color recording [17,18], i.e., sensitization for red or near-infrared light by pre-illumination with visible blue or green light, and in particular by the technique of thermal fixing [19,20]. Thermal fixing is performed by writing a holographic grating at elevated temperatures of about 180 °C. At these temperatures positively charged ions become mobile and compensate for the generated electronic space charge field [21]. After the sample has been cooled down, a homogeneous illumination with visible light yields a quasi-stabilized fixed hologram.

A rather new application of LiNbO₃ waveguides are holographic gratings that can be recorded with light of the photo-sensitive blue and green spectral region and then be used with infrared light [22,23], where the material is no longer sensitive. Here channel waveguides for infrared light around 1.55 μm wavelength are of particular interest because of their use in optical communications and measurement systems. In particular, permanent reflection Bragg gratings can help to build up dense wavelength division multiplexing (DWDM) systems for optical communications, serve as highly spectral-selective mirrors in integrated distributed Bragg reflection (DBR) lasers in Er-doped LiNbO₃, or may be used to build optical sensors for temperature and electric field measurement, to detect gases or complex biological molecules. Such sensors make use of the narrow spectral resonance of the holograms, where the filter reflectivity is already changed for very small effective index changes of the guided light.

In this contribution, we will review the work on holographic reflection filters in Fe- and Cu-doped LiNbO₃ channel waveguides. In the following section, the different steps for preparation of photorefractive waveguides are described. Thereafter, techniques and experimental setups for holographic recording and readout of the gratings are explained. The last part presents typical experimental results of photorefractive properties and performance of

holographic reflection gratings in LiNbO₃ channel waveguides. This includes charge-transport properties of diffusion-doped LiNbO₃, fundamental filter properties, the possibilities for hologram multiplexing, wavelength tuning and electrical switching of the filters, and a discussion on the long-term stability of thermally-fixed gratings.

2 Sample Preparation

The fabrication of photorefractive channel waveguides in LiNbO₃ crystals consists of several steps that have to be performed in a clean environment. As substrate material, pieces of commercially available x- or y-cut LiNbO₃ wafers can be used. Typical dimensions are $7 \times 17 \text{ mm}^2$, which, after the necessary polishing of the endfaces, results in samples with a length of about 15 mm. The ferroelectric *c*-axis coincides with the propagation direction of the light and points along the longer side. Single mode waveguide fabrication is done by Ti in-diffusion. At first a thin Ti layer with a typical thickness of 100 nm is deposited onto the polished surface using electron beam evaporation. Then lithographic techniques are used to pattern the Ti film into narrow stripes with a width of 6 to 8 μm . For larger stripe widths or thicker evaporated Ti films, higher modes of the waveguide can appear, and in this case more than one filter resonance will be observed. Typical parameters for Ti in-diffusion is an annealing time of 22 hours at a temperature of 1000 °C in air. In this way single mode waveguides for 1.55 μm wavelength with losses as low as 0.08 dB/cm are formed. They guide one TE and one TM mode which are both ordinarily polarized. An optimization of the waveguide parameters results in almost equal propagation constants of the two guided modes. This is of great importance for the filter performance because in this case the peak wavelength of the filter does not depend on input polarization. Furthermore, the size of the light field distribution of the single mode channel waveguides matches well with the typical diameter of non-polarizing single mode fibers for 1.55 μm , and a field overlap for direct fiber-chip coupling higher than 0.9 can be obtained in this way.

Doping of the surface layer is done by in-diffusion of thin films of either metallic Fe or Cu [15,16]. Layers of 5 to 100 nm thickness are evaporated onto the sample surface and in-diffused for several hours at temperatures of 1000 °C. The in-diffusion process can be either performed in Ar atmosphere to reduce the crystals, i.e., to get a larger ratio of Fe^{2+}/Fe^{3+} and Cu^+/Cu^{2+} , respectively, or it can be performed in O₂ atmosphere to get a smaller ratio. The diffusion constants of Fe and Cu into LiNbO₃ at a temperature of 1000 °C are $D_{Fe} = (1.8 \pm 0.2) \times 10^{-3} \mu\text{m}^2\text{s}^{-1}$ and $D_{Cu} = (1.0 \pm 0.2) \mu\text{m}^2\text{s}^{-1}$ [15,16]. Both are much larger than the value for Ti which is only $D_{Ti} = (4.4 \pm 0.5) \times 10^{-5} \mu\text{m}^2\text{s}^{-1}$ [15]. As a consequence, Cu doping of the sample surface has to be performed after the channel waveguides are fabricated by Ti in-diffusion, whereas Fe doping can be done also before this step. In both cases, a nearly

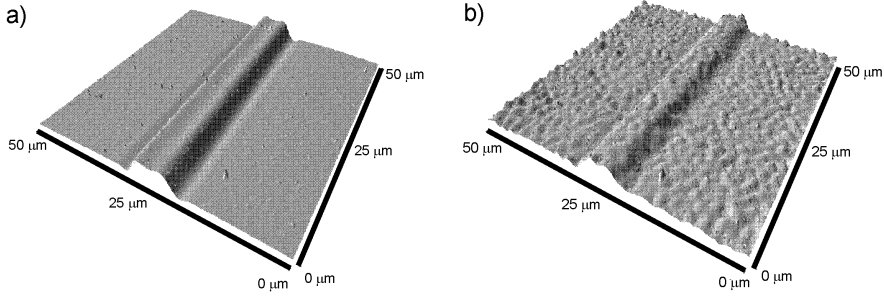


Fig. 1. Surface profiles of LiNbO₃:Ti:Cu channel waveguides measured with an AFM. Shown is a part of the 8 μm -wide channel for a sample with (a) $c_{\text{Cu}} = 1.1 \times 10^{25}$ atoms/m³ and (b) $c_{\text{Cu}} = 4.7 \times 10^{25}$ atoms/m³. The increase in height is due to the Ti in-diffusion into the sample and has an amplitude of about 200 nm

constant doping profile of either Fe or Cu is obtained in the range of the waveguide depth. This depth is defined by the Ti diffusion profile.

Typical doping concentrations in the waveguiding layer are in the range of 1 to 6×10^{25} atoms/m³ for Fe and 0.4 to 6×10^{25} atoms/m³ for Cu, respectively [22,24]. However, there exists a practical threshold for the amount of Cu that can be in-diffused into the surface of the substrate. For thicker layers of the evaporated Cu, diffusion leads to a decrease of surface quality and an increased Cu²⁺ absorption at 1.55 μm . As a result, the damping coefficient of the infrared light that is guided in the channel waveguides can be significantly increased, which may decrease the performance of the component or even prevent its applicability. As an example, in Fig. 1 surface scans of two different Cu-doped samples, measured with an atomic force microscope (AFM), are shown [24]. For lower doping ($c_{\text{Cu}} = 1.1 \times 10^{25}$ atoms/m³) the surface is still smooth and almost comparable to a sample without additional doping. When the doping is further increased ($c_{\text{Cu}} = 4.7 \times 10^{25}$ atoms/m³), surface roughness strongly increases. For samples with such a high Cu doping, the damping for 1.55 μm reaches values of 2 dBcm⁻¹. On the other hand, no degradation of the surface or increase of absorption in the infrared is observed for Fe in-diffusion.

Finally, the two endfaces of the waveguide sample have to be polished to enable direct light coupling with optical fibers. After this step the typical length d of the waveguide is about $d = 15$ mm. To increase the coupling efficiency into the waveguide and to reduce multiple reflections of the recording light inside the sample, anti-reflection coatings for the two endfaces and for the bottom face can be used. Although the refractive index of MgF₂ with $n_{\text{F}} = 1.34$ (for $\lambda = 1.55 \mu\text{m}$) does not match perfectly to the desired index of an ideal $\lambda/4$ -coating ($n_{\text{F}} \approx 1.49$), this material produces very resistant layers which adhere well on LiNbO₃ without additional heating. Such an annealing treatment has to be avoided in most cases, because otherwise it changes the

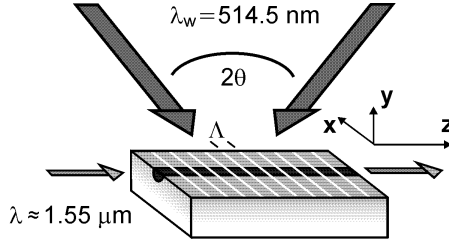


Fig. 2. Scheme of the recording and readout geometry for the holographic measurements. The gratings recorded with green light form reflection gratings for the infrared readout light in the channel waveguides

preset oxidation state of the in-diffused dopant (Fe or Cu). A 290 nm-thick layer of MgF₂ is used as an anti-reflection coating of the endfaces for infrared light. In the same way, a 110 nm-thick layer can be used to reduce the surface reflections of the green light during holographic recording.

3 Holographic Recording and Readout

In this section, we briefly describe the experimental setups for holographic recording and readout of the gratings, as well as the techniques for thermal fixing and development.

In principle, elementary refractive-index gratings can be written by two guided beams counter-propagating in the waveguide channel. However, as our samples are not sensitive to infrared light, gratings have to be recorded in the waveguide volume by two external beams of shorter wavelength that impinge upon the surface of the sample. This geometry is of advantage here, because it enables to adjust the grating period of the hologram by precisely choosing the correct intersection angle of the recording beams. A scheme of the recording and readout geometry is shown in Fig. 2. Two expanded light beams of the green line ($\lambda_w=514.5$ nm) of an Ar ion laser interfere inside the sample. The grating vector $K = 2\pi/\Lambda$ is directed along the c-axis and the recording light is ordinarily polarized to reduce holographic scattering and beam fanning. For the grating period we get

$$\Lambda = \lambda_w / (2 \sin \Theta) , \quad (1)$$

where 2Θ is the (full) intersection angle of the two beams outside the sample. With an angle of $2\Theta \approx 90^\circ$, readout of the gratings in a linear reflection geometry is possible using (guided) infrared light with a wavelength around 1.55 μm .

Thermal fixing is performed by heating the waveguide sample to 180 °C while the grating is written [19,20]. In this way, positively charged ions (e.g., protons) become mobile and can compensate for the generated electronic space-charge field [21]. Because of the relatively long recording times of up to 2 hours an active phase stabilization has to be used [22,26,27]. This system compensates for thermal drift of the sample holder and other optical components and thus ensures a stable light pattern during recording.

Special care has to be taken to precisely adjust the angle 2Θ during recording, because this defines the position of the peak wavelength λ_p for readout of the grating:

$$\lambda_p = 2n_{\text{eff}}(T, c_{\text{Fe/Cu}})\Lambda(T, \Theta) . \quad (2)$$

Although the effective refractive index n_{eff} of the guided light is predominantly defined by the diffusion profile of Ti which is constant for all samples investigated here, both Fe and Cu doping results in a slightly shifted value of n_{eff} [15,24]. Next, the thermal expansion of LiNbO₃ at higher temperatures T must be taken into account, too, because this directly changes the grating period Λ [23]. We can roughly estimate that the peak wavelength λ_p of a grating recorded at 180 °C is reduced by 1 nm when the sample is cooled down to room temperature. Last, the refractive indices of LiNbO₃ depend on temperature, but for the ordinary index that is used here this influence can be neglected when compared with the effect of thermal expansion.

After recording the samples are cooled down to room temperature within a few minutes. The fixed gratings can be developed by homogeneous illumination with the expanded light beam of an Ar ion laser. Alternatively, incoherent light of a halogen lamp can be used. The holograms are read in reflection geometry in the waveguide channels with the guided, ordinarily polarized TE and/or TM mode. In the following we have used a DFB laser which can be tuned over a small wavelength range around 1557 nm. At the peak wavelength λ_p the Bragg condition for readout, $\Lambda = \lambda_p/2n_{\text{eff}}$, is exactly fulfilled, and the transmission drops down from unity to a minimum at $T(\lambda_p) = 1 - \eta$. The diffraction efficiency η at the peak wavelength λ_p is given by the Kogelnik equation [25]

$$\eta(\lambda_p) = \tanh^2(\pi\Delta n d/\lambda_p) . \quad (3)$$

Here Δn is the amplitude of the refractive index change and d is the grating length.

4 Experimental Results

In this section the experimental results of sample characterization will be summarized. At first we present some fundamental properties of the photorefractive Ti in-diffused waveguides in LiNbO₃. Then the recorded holographic filters will be analyzed and the possibilities for hologram multiplexing, thermal tuning of peak wavelengths, and electrical switching of the filter will be discussed. The last part describes the influence of dark compensation on the grating relaxation, i.e., long-term stability of the gratings. Moreover, a new method for thermal fixing that does not need any further development process will be introduced.

4.1 Photorefractive Properties

For optimization of the filter properties a detailed knowledge of the charge transport mechanism and fundamental photorefractive properties of the waveguide samples is necessary. Here results from volume-doped crystals may be not simply transferred because of the high Ti concentration in the waveguiding layer, and, especially for some of the samples, high doping level with either Fe or Cu. Furthermore, the doping process by in-diffusion of metal layers instead of doping during growth of the crystals, may result in different impurities sites in the crystal lattice, which can influence the charge transport properties, too.

Light-induced refractive-index changes can be measured by recording of holographic gratings at room temperature. If gratings are written for different recording times t , the saturated refractive-index change Δn_s can be obtained by fitting an exponential function of the form

$$\Delta n(t) = \Delta n_s [1 - \exp(-t/\tau)] \quad (4)$$

to the measured data $\Delta n(t)$. An example for different Cu-doped samples is given in Fig. 3(a). When plotting the saturated refractive-index change Δn_s as a function of Cu concentration c_{Cu} of different samples in Fig. 3(b), a linear dependence is found. We can assume an almost constant ratio $c_{\text{Cu}^+}/c_{\text{Cu}^{2+}}$ for all the investigated waveguides, because all samples have been thermally treated in the same way during fabrication. This assumption leads to a linear dependence $\Delta n_s \propto c_{\text{Cu}^{2+}}$, which is in agreement with a one-center model of charge transport [28].

The photoconductivity of the photorefractive waveguides can be determined by measuring the decay of the gratings during homogeneous light illumination. First holographic gratings are written at room temperature with green light, and the diffraction efficiency η and the peak wavelength λ_p for, e.g., TM-polarized infrared light are measured. Then the sample is illuminated homogeneously off-Bragg with green light, and in time intervals of a few seconds the diffraction efficiency at the peak wavelength is determined again. The temporal development of refractive-index change $\Delta n(t)$ is obtained using the Kogelnik equation in Eq. (3), see Fig. 4(c). From this dependence we can calculate the photoconductivity σ_{ph} using the relations

$$\Delta n(t) = \Delta n^0 \exp(-t/\tau) , \quad (5)$$

$$\sigma_{\text{ph}} = \epsilon \epsilon_0 / \tau . \quad (6)$$

Here Δn^0 is the refractive-index change for $t = 0$, ϵ_0 is the permittivity of free space, and $\epsilon = 28$ is the appropriate dielectric constant of LiNbO₃. In Fig. 4(d) the photoconductivity σ_{h} is given as a function of the erasure intensity I ($\lambda = 514.5$ nm) for different Cu-doped samples. As can be seen, photoconductivity depends linearly on intensity, $\sigma_{\text{ph}} \propto I$, which is again in good agreement with a one-center model for charge transport. The absolute

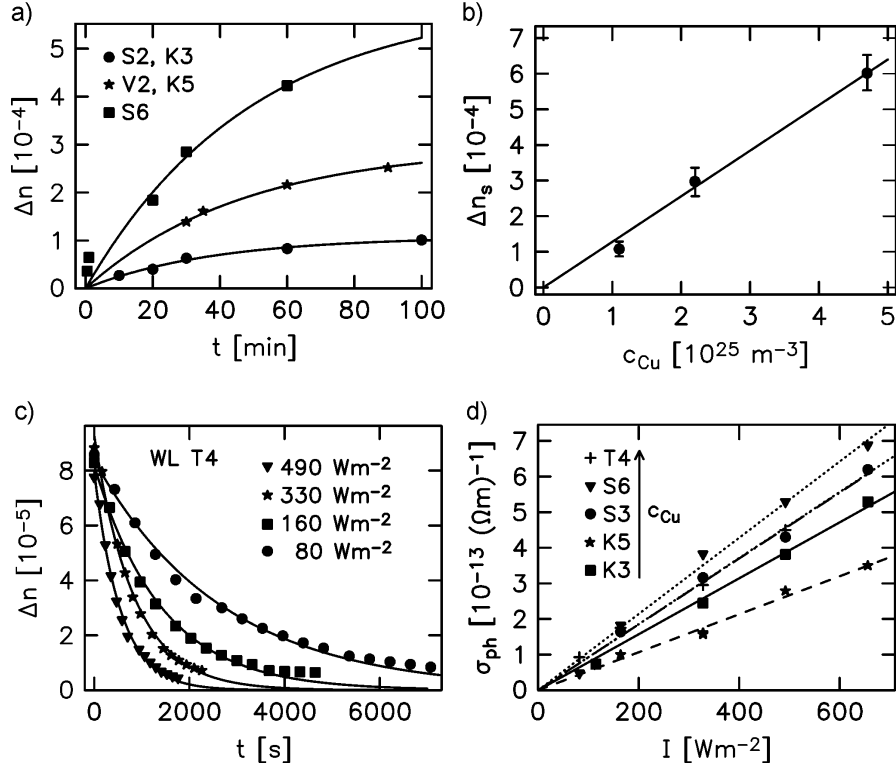


Fig. 3. Light-induced refractive-index changes and photoconductivity in Cu-doped LiNbO₃ waveguides recorded at room temperature: **(a)** Refractive-index change Δn versus recording time t for different samples (S2/K3: $c_{Cu} = 1.1 \times 10^{25} \text{ m}^{-3}$; V2/K5: $c_{Cu} = 2.2 \times 10^{25} \text{ m}^{-3}$; S6: $c_{Cu} = 4.7 \times 10^{25} \text{ m}^{-3}$), **(b)** saturated refractive-index change Δn_s versus copper concentration c_{Cu} , **(c)** decay of refractive-index gratings Δn because of homogeneous illumination with green light ($\lambda_w = 514.5 \text{ nm}$) of varying intensity for the sample T4 ($c_{Cu} = 5.7 \times 10^{25} \text{ m}^{-3}$), and **(d)** photoconductivity σ_{ph} as a function of erasure intensity I for different Cu-doped samples (S3: $c_{Cu} = 3.2 \times 10^{25} \text{ m}^{-3}$)

value of the specific photoconductivity σ_{ph}^o , defined by $\sigma_{ph}^o = \sigma_{ph}/I$, is of the order of some 10^{-16} mV^{-2} , which is comparable to data obtained for homogeneously copper-doped volume samples [29]. Fe-doped LiNbO₃ waveguides have been investigated as well, and for this dopant a good agreement of the photorefractive properties with the predictions of a one-center model has been obtained, too.

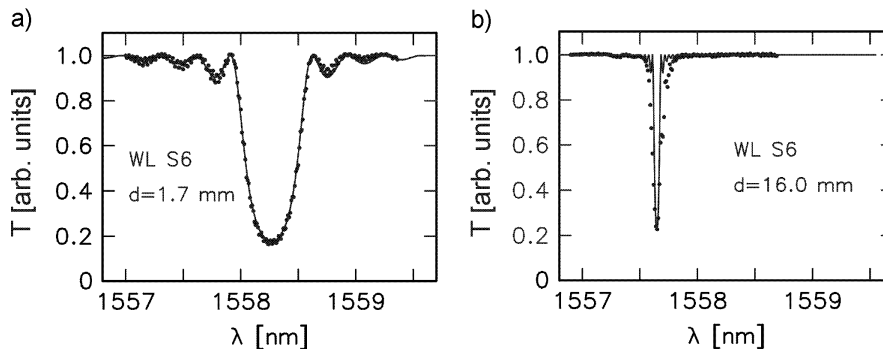


Fig. 4. Transmission T versus wavelength λ for gratings recorded at room temperature in LiNbO₃:Ti:Cu channel waveguides: (a) grating length $d = 1.7$ mm, recording time 60 min; (b) grating length $d = 16.0$ mm, recording time 1 min. The solid lines are fits of the wavelength-dependent Kogelnik equation [25]

4.2 Fundamental Filter Properties

Next we will discuss some principal properties of holographic reflection gratings in channel waveguides. The following examples have been obtained in Cu-doped samples, where gratings were recorded with green light and a total writing intensity of 1200 Wm^{-2} . Recording has been performed at room temperature, so the gratings are not thermally fixed. The length d of a grating can be simply adjusted by using an additional aperture (slit) for the recording light placed directly on top of the surface of the waveguide. In Fig. 4(a) and 4(b) the filter characteristics for a short ($d=1.7$ mm, writing time 60 min) and for a long grating ($d=16$ mm, writing time 1 min), respectively, are presented. For better comparison, the recording times have been adjusted to get almost equal diffraction efficiencies of about 80% at the respective peak wavelength. As expected, the full-width-half-minimum (FWHM) is strongly decreased for longer gratings and can reach values as low as 0.05 nm. The transmission curves $T(\lambda)$ ("rocking curves") are also in fairly good agreement with the predictions of the wavelength-dependent Kogelnik equation in [25], which are plotted as solid lines in the two graphs with Δn as a free parameter.

Gratings can be read with both, TE- or TM-polarized infrared light. For our standard channel waveguide parameters (6 μm -wide channel, diffusion of a 100 nm-thick Ti layer for 22 h at 1000 °C) and Fe doping we get almost identical effective refractive indices of the the two modes. In this way, a nearly polarization independent filter can be realized. Here the difference of the corresponding peak wavelengths for the two polarizations of the order of 0.05 nm. It can be completely eliminated by applying a small bias voltage to the sample and tuning the effective refractive indices via the electrooptic effect.

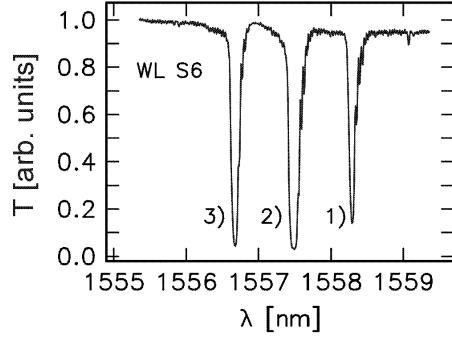


Fig. 5. Three superimposed reflection gratings for infrared light in a LiNbO₃:Ti:Cu channel waveguide. Shown is the normalized transmission T versus readout wavelength λ . The hologram spacing is 0.8 nm with an average diffraction efficiency of about 93 %

The filter characteristic can be further tailored, for instance to get nearly rectangular transmission curves $T(\lambda)$, by using both, chirped and apodized gratings. Simple chirped gratings can be fabricated by using slightly curved wave fronts instead of plane waves for recording. More complicated gratings can be realized with the help of specially-designed phase masks through which the samples are illuminated during recording with a single laser beam [10]. At the same time, the use of phase masks will result in a recording geometry that is less sensitive to phase fluctuations and instabilities, and thus may be a good alternative for the two-beam holographic setup that has been described in the preceding section. However, the freedom to adjust the grating period(s) by simply changing the recording angle will be lost in this way. Apodization of the holograms can be realized in different ways. The grating can be written with a locally-varying intensity distribution, which then results in a locally-varying refractive-index change, too. Another possibility is to use a non-homogeneous illumination for the development of the gratings.

4.3 Hologram Multiplexing

In photorefractive crystals several holograms can be superimposed in the same volume, and they can be addressed either by changing the angle under which the readout beam enters the sample, or by tuning the readout wavelength. The latter option has to be used for holographic gratings in a linear reflection geometry, i.e., for channel waveguides. Here several gratings with different grating periods can be recorded and thermally fixed, thus reflecting several wavelengths at the same time.

To demonstrate the multiplexing capabilities of photorefractive channel waveguides in LiNbO₃, three reflection holograms with a peak spacing of 0.8 nm, corresponding to a 100 GHz channel spacing in DWDM, are superimposed in a Cu-doped sample. The resulting transmission spectrum for TM polarization is plotted in Fig. 5. The holograms are recorded at room temperature one after the other. To compensate for the erasure of the first and second hologram during recording of the latter ones, the respective recording times have to be properly adjusted. In the example here they decrease from

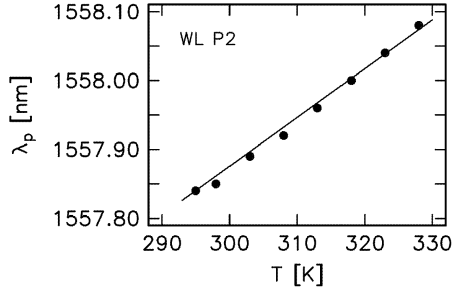


Fig. 6. Peak wavelength λ_p versus sample temperature T_s of a fixed grating in a LiNbO₃:Ti:Fe channel waveguide. A linear fit (solid line) yields the thermal expansion coefficient $\alpha_{33} = (4.5 \pm 0.5) \times 10^{-6} \text{ K}^{-1}$

16 min for the first hologram (1) to 4 min and 1.5 min for the second (2) and third (3) one, respectively, resulting in an average diffraction efficiency of about 93 % for each hologram. The length of the gratings was approximately 16 mm.

4.4 Wavelength Tuning and Electrical Switching

The position of the peak wavelength λ_p of a holographic filter depends on both, the grating period Λ and the effective refractive index n_{eff} of the guided light. Therefore, the filter properties can be tuned by heating the sample, i.e., by thermal expansion, or by applying external electric fields, i.e., using the electrooptic effect:

$$\lambda_p(T_s) = \lambda_p(T_0)(1 + \alpha_{33}(T_s - T_0)) , \quad (7)$$

$$\lambda_p(E) = \lambda_p(E = 0)(1 - 0.5 n_{\text{eff}}^2 r_{22} E) , \quad (8)$$

where $(T_s - T_0)$ is the difference of sample and reference temperature, α_{33} is the thermal expansion coefficient along the c -axis, E is the applied electric field along the y -axis, and $r_{22} = -r_{12}$ is the appropriate electrooptic tensor element. While thermal effects, due to its relatively large response time, are well suited for precise tuning of the peak wavelength, the fast response of the electrooptic effect can be used for switching on and off the filter.

Fig. 6 presents a measurement of the peak wavelength λ_p of a fixed grating in a LiNbO₃:Ti:Fe channel waveguide as a function of the sample temperature T_s . The minimum of the transmitted spectrum $T(\lambda)$ for TM polarization has been evaluated. Obviously, the data follow a straight line, and from a linear fit the thermal expansion coefficient $\alpha_{33} = (4.5 \pm 0.5) \times 10^{-6} \text{ K}^{-1}$ can be determined. Here we have neglected the temperature dependence of the effective refractive index n_{eff} for the infrared light in the investigated temperature range.

4.5 Long-Term Stability of Fixed Gratings

The lifetime of thermally-fixed refractive-index gratings is an important factor for the application of integrated holographic filters. A drawback of these

devices, when compared with photorefractive volume samples, are the high concentration of Ti in the waveguiding layer, as well as the high doping level of either Fe or Cu that is required to obtain diffraction efficiencies close to 100 %. High impurity concentrations lead to a significant increase of the dark conductivity, which in turn causes a relaxation of the thermally-fixed and developed holographic gratings.

For samples with no doping or very low doping level, dark conductivity is mainly caused by proton conductivity. However, for higher Fe- and Cu-doped LiNbO₃ bulk samples and waveguides, dark conductivity is dominated by the influence of impurities and increases exponentially with doping concentration. Thermally excited electrons can drift in the ionic space-charge field, which finally leads to an almost complete compensation of this field with no net refractive-index change.

In most of the Fe- and some of the Cu-doped samples such a relatively fast dark-relaxation of the fixed gratings is observed. As an example, this effect is shown in Fig. 7 for a grating in a LiNbO₃:Ti:Fe channel waveguide. This sample has a dark conductivity of $\sigma_d \approx 2.0 \times 10^{-16} \Omega^{-1}\text{m}^{-1}$, which causes a relaxation of the refractive-index change with a time constant of about 50 hours. On the other hand, the grating can be re-developed by homogeneous illumination. Despite of the option of a complete re-development, the refractive-index change can be adjusted to any desired value $\Delta n' < \Delta n_s$ by permanent illumination of the sample with light of low intensity, e.g., using blue LED's. With such an illumination, at a certain level of relaxation that is due to dark conductivity, a balance of dark relaxation and grating development can be reached, i.e., the electronic drift current is compensated by a photovoltaic current generated by the illumination. This effect is shown in Fig. 7 for different intensities of the blue light ($\lambda = (494 \pm 10) \text{ nm}$) filtered out of the spectrum of a halogen lamp with an interference filter. Using the same mechanism but with a non-homogeneous illumination of the sample, it is possible to fabricate apodized gratings with spatially-varying amplitude of the refractive-index change.

An interesting and for applications important observation has been made during the investigation of reduced Cu-doped waveguides [31]. In these samples, thermally-fixed gratings have been recorded that do not need any development process and that are stable in the dark, i.e., they do not suffer from relaxation because of the high dark conductivity. This effect will be discussed in detail in the following section. In a first experiment, a reflection grating has been recorded for 60 min in the oxidized waveguide W3 at a temperature of 180 °C. Thereafter, when the sample has been cooled down to room temperature, the corresponding transmission spectrum $T(\lambda)$ was taken in the infrared. Fig. 8(a) shows this spectrum at the initial stage directly after recording. In Fig. 8(b) the spectrum after the grating has been developed by homogeneous illumination with intensive green light is displayed. Without development, only a very small Bragg peak can be seen, which is

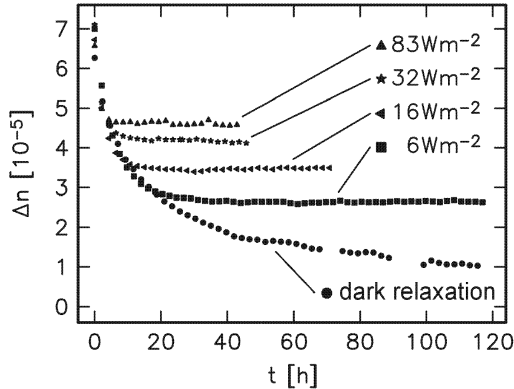


Fig. 7. Compensation of a fixed grating in LiNbO₃:Ti:Fe in the dark and under illumination with incoherent blue light ($\lambda = (494 \pm 10)$ nm). Shown is the temporal evolution of the refractive-index change Δn for different intensities and in the dark. After each measurement the hologram has been re-developed up to saturation using intensive green light

in good agreement with the behavior expected from the common theory of thermal fixing in LiNbO₃ [19–21]. When the fixed hologram is developed until saturation by homogeneous illumination, the reflection efficiency increases dramatically. From the measured diffraction efficiency of $\eta = 98.5\%$ for the infrared light we can calculate a refractive-index change of $\Delta n = 1.2 \times 10^{-4}$ in the waveguiding channel by using Eq. (3).

The same measurement has been repeated with the reduced waveguide T4. In this sample, the copper concentration is more than two times higher as in W3, and the ratio $c_{\text{Cu}^+}/c_{\text{Cu}^{2+}}$ is much larger. A grating has been recorded for 120 min at 180 °C, and again, directly after cooling down, the transmission spectrum has been examined. As can be seen in Fig. 8(c), a strong peak is identified and the measured diffraction efficiency reaches 95.6%, corresponding to a refractive-index change of about $\Delta n = 8 \times 10^{-5}$. It should be emphasized that at this stage no development of the grating has been performed. Then the fixed grating in this sample is additionally developed with green light. The measured spectrum is given in Fig. 8(d), where the maximum reflection efficiency is now considerably decreased to a value of 50.2%.

The corresponding temporal behavior of the refractive-index change $\Delta n(t)$ during development is non-monotonous: the value of Δn first rapidly drops down, then passes through a minimum and finally reaches a steady-state value that is still much smaller than the initial value Δn^0 . The completely developed refractive-index grating of the reduced sample T4 has been kept at room temperature in the dark and the temporal evolution of Δn was again monitored over a total range of 250 hours. The result is given in Fig. 9 and shows the reverse process: Δn first decreases, passes through a minimum and grows again before it finally saturates. Now the saturation value is larger than the start value. In the dark Δn evolves back to its initial value Δn^0 before the development process. In the dark (without development) the initial refractive-index changes Δn^0 are stable, and no decrease is measured for a time of more than one year.

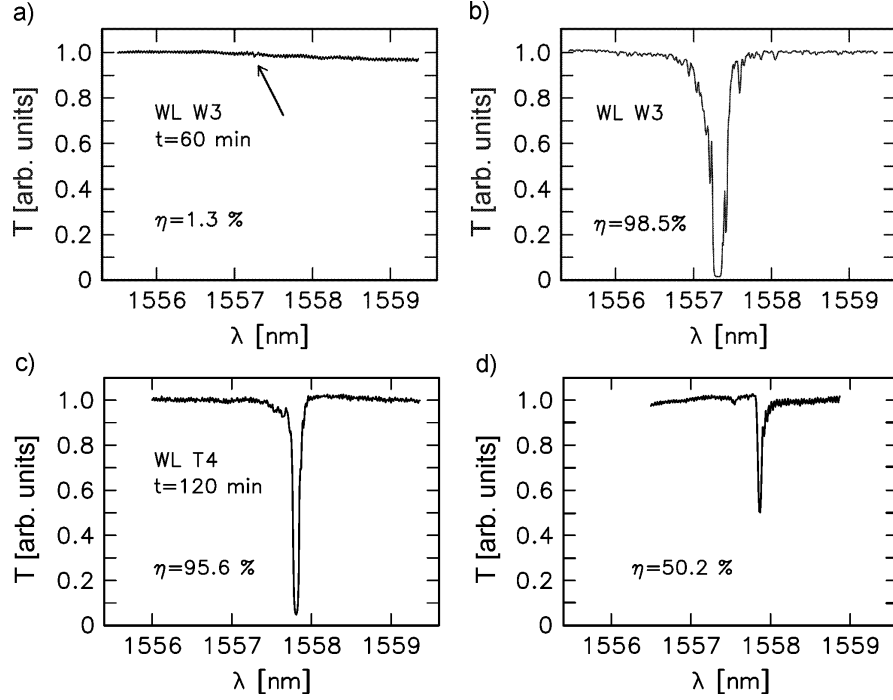


Fig. 8. Transmission T before ((a) and (c)) and after ((b) and (d)) the development process versus readout wavelength λ for gratings recorded in the Cu-doped, oxidized sample W3 (upper plots (a)/(b); recording time 60 min) and in the Cu-doped, reduced sample T4 (lower plots (c)/(d); recording time 120 min). For the oxidized sample, the development leads to an increase of diffraction efficiency from 1.3 % to 98.5 %, whereas for the reduced sample a decrease of diffraction efficiency from 95.6 % to 50.2 % is measured after development. The oxidized sample with $c_{\text{Cu}} = 2.2 \times 10^{25} \text{ m}^{-3}$ has been annealed in dry O₂ atmosphere, while the reduced one with $c_{\text{Cu}} = 5.7 \times 10^{25} \text{ m}^{-3}$ has been annealed in wet Ar atmosphere

For an explanation of the observed temporal evolution of Δn we assume a superposition of two different refractive-index gratings Δn_b and Δn_c that are out of phase by $(180^\circ - \phi)$. The corresponding model is illustrated in Fig. 10. The grating Δn_c grows already during high temperature recording and remains constant after cooling down. At room temperature it is not affected by light anymore. The second grating Δn_b is generated during the development process. It grows exponentially until saturation with a time constant τ_1 while the sample is illuminated homogeneously. The time evolution of the refractive-index change is thus described by

$$n(t) = \left([\Delta n_c - \Delta n_b^0 \cos \phi (1 - \exp(-t/\tau_1))]^2 + [\Delta n_b^0 \sin \phi (1 - \exp(-t/\tau_1))]^2 \right)^{-\frac{1}{2}}. \quad (9)$$

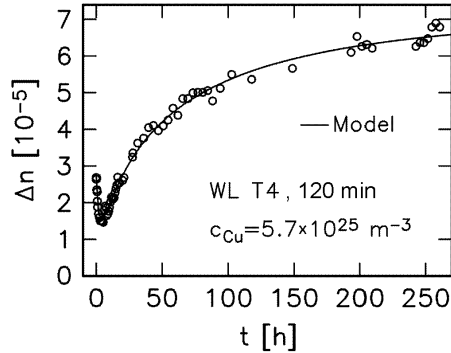


Fig. 9. Dark compensation of a fixed and developed grating in a reduced LiNbO₃:Ti:Cu channel waveguide. Shown is the temporal development of the refractive-index change Δn . The solid line is a fit according to Eq. (10)

Correspondingly, the time evolution of the refractive-index change in the dark can be described by

$$n(t) = \left(\left[\Delta n_c - \Delta n_b^0 \cos \phi \exp(-t/\tau_2)^\gamma \right]^2 + \left[\Delta n_b^0 \sin \phi \exp(-t/\tau_2)^\gamma \right]^2 \right)^{-\frac{1}{2}}, \quad (10)$$

with τ_2 for the time constant for erasure of the grating Δn_b and γ as the exponent of a stretched exponential [30].

From the time evolution of Δn_b we can deduce that this grating is mainly connected to the photovoltaic effect. This is the dominating mechanism for charge redistribution in doped LiNbO₃. Because during thermal fixing the space-charge field is permanently compensated by screening ions that are mobile at high temperatures, a deep modulation of the Cu⁺ traps arises. Then, when the sample is cooled down to room temperature, a homogeneous light illumination generates modulated photocurrents, and the grating Δn_b appears. After the development process the photovoltaic grating Δn_b is slowly erased via the dark conductivity of the material, and the temporal development of this dark erasure can be described by a stretched exponential function [30]. Furthermore, a small diffusion grating is present that has a phase difference of 90° to the photovoltaic grating. This results in the small phase difference ϕ from the exact out-of-phase condition of 180° of Δn_b relative to the grating with amplitude Δn_c .

Most likely the permanent grating Δn_c is attributed to a redistribution of Cu ions. This conclusion is based on the fact that the measured permanent gratings are uniquely found in samples that are doped with Cu and have never been observed in Fe-doped samples. This is also the reason why we can neglect a modulated proton concentration as the origin of this permanent grating. We can also rule out that this effect results from an absorption grating formed during the recording process, because the efficiency of such a grating is much smaller (limited to $\eta < 7.2\%$ [25]) than that observed in our samples. There are two possibilities for the Cu ions to generate the grating Δn_c . First the deep modulation of the Cu⁺ and Cu²⁺ ions can already lead to ma-

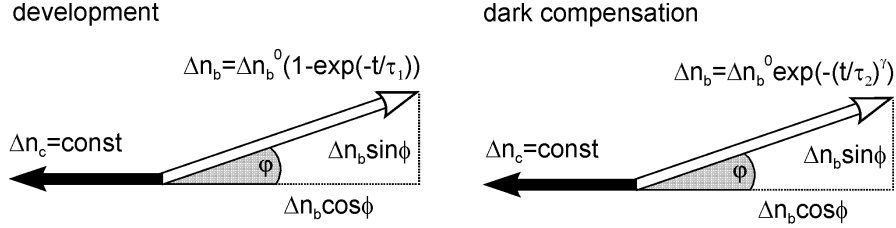


Fig. 10. Model for the refractive-index evolution during the development process and in the dark for reduced Cu-doped waveguides

terial changes that cause a measurable refractive-index change, and second, it is not established that protons, like in LiNbO₃:Fe, are responsible for the compensation of the space-charge field during thermal fixing in LiNbO₃:Cu [21]. It may be possible that Cu ions move in the space-charge field during holographic recording and thus lead to material and density changes that may cause the observed additional refractive-index changes. This means that the Cu concentration itself will be modulated during fixing, not only the distribution of the Cu⁺ and the Cu²⁺ ions alone.

5 Conclusions and Outlook

In this contribution we have reported on the formation of fixed reflection gratings in photorefractive Fe- and Cu-doped, Ti in-diffused LiNbO₃ channel waveguides for infrared light. Holographic gratings are recorded with visible light of an Ar ion laser at high temperatures of 180 °C. The gratings can be read with guided infrared light around 1.55 μm, and strong refractive-index modulations are obtained. By choosing the appropriate waveguide parameters and an optimization of the diffusion process, nearly polarization-independent holographic filters with efficiencies close to 100 % and a bandwidth (FWHM) as low as 0.05 nm are obtained. Several of such filters with different reflection wavelengths can be superimposed in the same waveguide sample. This enables the fabrication of more complicated filters for DWDM, or for optical sensors that make use of the narrow spectral resonance. We have proven the possibility to thermally adjust the peak wavelength of a reflection grating in a range of some tenths of nanometers, and the experimental verification of electrical switching of filters via the electrooptic effect is currently under investigation.

For commercial applications of thermally-fixed waveguide filters, or similar devices in photorefractive bulk samples that also require a fixation process, special care has to be taken to ensure a long-term stability of the holograms. In this sense, very promising results have been obtained for reduced Cu-doped LiNbO₃. In these samples, large refractive-index changes appear without the need of any additional development process. These strong refractive-index

modulations do, most likely, not originate from the photorefractive effect but from material changes, i.e., density changes that are caused by a migration of Cu ions because of the electronic space-charge field. Such gratings are stable in the dark for at least one year with no degradation, and no compensation mechanism via dark conductivity is observed. On the other hand, a drawback of these samples is the increased absorption at 1.55 μm because of the strong Cu doping. However, we believe that these new result will stimulate the further development and application of devices based on photorefractive crystals in optical communications and integrated optics.

References

1. T. Tamir (Ed.): Guided-wave optoelectronics (Springer, Berlin 1990)
2. A.M. Prokhorov, Y.S. Kuzminov: Physics and chemistry of crystalline lithium niobate, Adam Hilger Series in Optics and Optoelectronics, E.R. Pike, R.G.W. Brown (Eds.), (Adam Hilger, New York 1990)
3. A.M. Prokhorov, Y.S. Kuzminov, O.A. Khachatryan: Ferroelectric thin-film waveguides in integrated optics (Cambridge International Science, Cambridge 1996)
4. R.V. Schmidt, I.P. Kaminov: Metal-diffused optical waveguides in LiNbO₃, Appl. Phys. Lett. **25**, 458-460 (1974)
5. J.L. Jackel, C.E. Rice, J.J. Veleka: Proton exchange in LiNbO₃, Ferroelectr. **50**, 165-170 (1983)
6. V.E. Wood, P.J. Cressman, R.L. Holman, C.M. Verber: Photorefractive effects in waveguides, in *Photorefractive Materials and Their Applications II*, P. Günter, J.-P. Huignard (Eds.), Topics in Applied Physics Vol. 62 (Springer, Berlin, Heidelberg 1988)
7. D. Kip: Photorefractive waveguides in oxide crystals: fabrication, properties, and applications, Appl. Phys. B **67**, 131-150 (1998)
8. R.C. Alferness, R.V. Schmidt, E.H. Turner: Characteristics of Ti-diffused lithium niobate optical directional couplers, Appl. Opt. **18**, 4012-4016 (1979)
9. W.K. Burns, A.B. Lee, A.F. Milton: Active branching waveguide modulator, Appl. Phys. Lett. **29**, 790-792 (1976)
10. C. Becker, A. Greiner, T. Oesselke, A. Pape, W. Sohler, H. Suche: Integrated optical Ti:Er:LiNbO₃ distributed Bragg reflector laser with a fixed photorefractive grating, Opt. Lett. **15**, 1194-1196 (1998)
11. W. Sohler, H. Suche: Erbium doped lithium niobate waveguide devices, in *Design and Application of Integrated Optical Circuits and Components*, E. Murphy (Ed.), (Marcel Decker, Inc. 1999)
12. F.S. Chen, J.T. LaMacchia, D.B. Fraser: Holographic storage in lithium niobate, Appl. Phys. Lett. **13**, 223-225 (1968)
13. A. Askin, G.D. Boyd, J.M. Dziedzic, R.G. Smith, A.A. Ballman, J.J. Levinstein, K. Nassau: Optically-induced refractive index inhomogeneities in LiNbO₃ and LiTaO₃, Appl. Phys. Lett. **9**, 72-74 (1966)
14. P. Günter, J.-P. Huignard (Eds.): Photorefractive Materials and Their Applications I + II, Topics in Applied Physics Vol. 61 and 62 (Springer, Berlin, Heidelberg 1988)

15. D. Kip, B. Gather, H. Bendig, E. Krätzig: Concentration and refractive index profiles of titanium- and iron-diffused planar LiNbO₃ waveguides, *Phys. Status Solidi (a)* **139**, 241-248 (1993)
16. J. Hukriede, D. Kip, E. Krätzig: Copper diffusion into lithium niobate, *Phys. Status Solidi (a)* **172**, R3 (1999)
17. L. Hesselink, S. Orlov, A. Liu, A. Akella, D. Lande, R. Neurganankar: Photorefractive materials for nonvolatile volume holographic data storage, *Science* **282**, 1089-1094 (1998)
18. J. Imbrock, D. Kip, E. Krätzig: Nonvolatile holographic storage in iron-doped lithium tantalate with continuous-wave laser light, *Opt. Lett.* **24**, 1302-1304 (1999)
19. J.J. Amodei, D.L. Staebler: Holographic pattern fixing in electrooptic crystals, *Appl. Phys. Lett.* **18**, 540-542 (1971)
20. H. Vormann, G. Weber, S. Kapphan, E. Krätzig, Hydrogen as origin of thermal fixing in LiNbO₃, *Sol. State Commun.* **40**, 543-545 (1981)
21. K. Buse, S. Breer, K. Peithmann, S. Kapphan, M. Gao, E. Krätzig: Origin of thermal fixing in photorefractive lithium niobate crystals, *Phys. Rev. B* **56**, 1225-1235 (1997)
22. J. Hukriede, D. Kip, E. Krätzig: Thermally fixed reflection gratings for infrared light in LiNbO₃:Ti:Fe channel waveguides, *Opt. Lett.* **23**, 1405-1407 (1998)
23. J. Hukriede, D. Kip, E. Krätzig: Thermal tuning of a fixed Bragg grating for IR light fabricated in a LiNbO₃:Ti channel waveguide, *Appl. Phys. B* **70**, 73-75 (2000)
24. J. Hukriede, D. Kip, E. Krätzig: Investigation of titanium- and copper-indiffused channel waveguides in lithium niobate and their application as holographic filters for infrared light, *J. Opt. A: Pure Appl. Opt.* **2**, 481-487 (2000)
25. H. Kogelnik: Coupled wave theory for thick hologram gratings, *Bell Syst. Tech. J.* **48**, 2909-2947 (1969)
26. P.M. Garcia, K. Buse, D. Kip, J. Frejlich: Self-stabilized holographic recording in LiNbO₃:Fe crystals, *Opt. Commun.* **117**, 235-240 (1995)
27. J. Frejlich, P.M. Garcia, A.A. Frechi: Deeply modulated stabilized photorefractive recording in LiNbO₃:Fe, *Opt. Mat.* **4**, 410-413 (1995)
28. K. Buse: Light-induced charge transport processes in photorefractive crystals I: models and experimental methods, *Appl. Phys. B* **64**, 273-291 (1997)
29. K. Peithmann, J. Hukriede, K. Buse, E. Krätzig: Photorefractive properties of lithium niobate volume crystals doped by copper indiffusion, *Phys. Rev. B* **61**, 4615-4620 (2000)
30. I. Nee, M. Müller, K. Buse, E. Krätzig: Role of iron in lithium niobate crystals for the dark-storage-time of holograms, *J. Appl. Phys.* **88**, 4282-4286 (2000)
31. J. Hukriede, D. Kip, E. Krätzig: Permanent narrow-band reflection holograms for infrared light recorded in LiNbO₃:Ti:Cu channel waveguides, *Appl. Phys. B* **72**, 749-753 (2001)